



Comparison of One-Part and Two-Part Alkali-Activated Metakaolin and Blast Furnace Slag

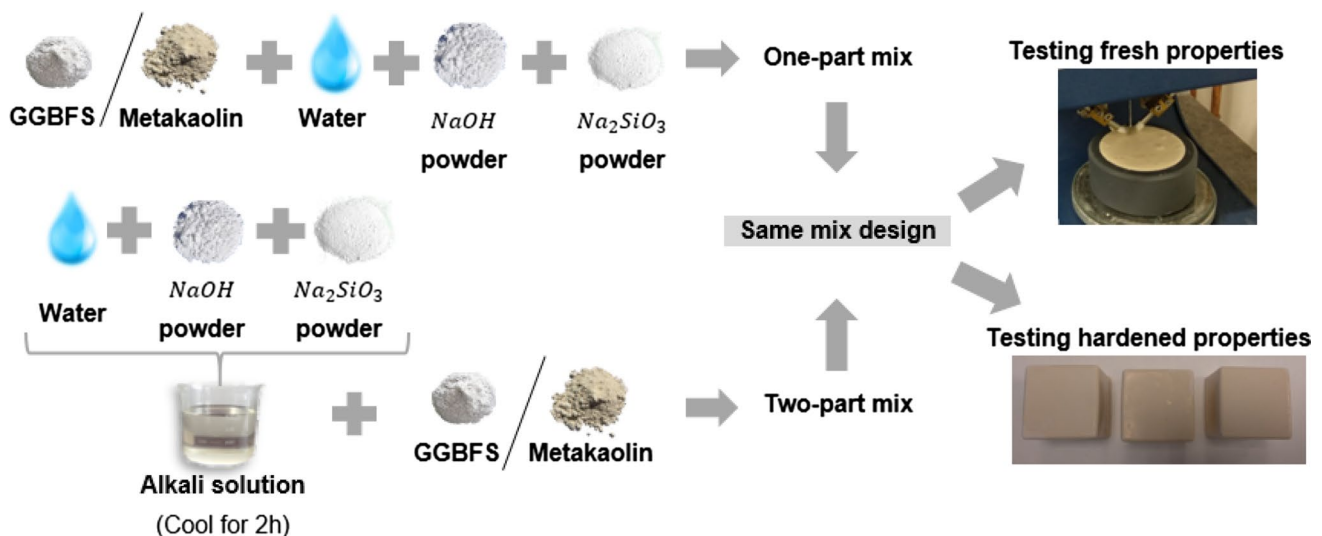
Isabel Pol Segura¹ · Tero Luukkonen² · Juho Yliniemi² · Harisankar Sreenivasan² · Anne Juul Damø¹ · Lars Skaarup Jensen³ · Mariana Canut³ · Anu M. Kantola⁴ · Ville-Veikko Telkki⁴ · Peter Arendt Jensen¹

Received: 21 June 2022 / Accepted: 26 September 2022 / Published online: 13 October 2022
© The Author(s) 2022

Abstract

One-part alkali-activated materials prepared with solid-form alkali activator are gaining attention in the construction industry, as they are an easier and safer approach for cast-in-situ applications in comparison with two-part approach (i.e., involving the use of alkali-activator solutions). The present study compares the one-part and conventional two-part mixing methods with two aluminosilicate precursors, metakaolin and ground granulated blast-furnace slag, using identical mix designs (in terms of molar ratios of SiO_2 , Al_2O_3 , and Na_2O) with both preparation methods. The results revealed that using one-part mix delays the setting time, increases the heat of reaction, decreases the shrinkage, and reaches between 80 and 85% of the compressive strength of the two-part mix. In addition, scanning electron microscopy, thermogravimetric analysis, and X-ray diffraction analysis showed no major differences between one- and two-part. However, energy-dispersive X-ray spectroscopy and magic angle spinning nuclear magnetic resonance experiments indicated that the extent of reaction in two-part alkali-activated mixes is higher than for one-part.

Graphical Abstract



Keywords One-part alkali activated · Two-part alkali activated · Metakaolin · Blast furnace slag

The contributing editor for this article was Mansoor Barati.

✉ Isabel Pol Segura
isapol@kt.dtu.dk

Extended author information available on the last page of the article

Introduction

Manufacturing of Ordinary Portland cement (OPC) contributes significantly to the global warming process, accounting approximately 7 to 8% of the global anthropogenic CO₂ emissions [1–3]. Moreover, it has been estimated that it could contribute up to 20% by 2050 due to the increasing cement demand [4]. The cement industry is working with different alternatives to lower the CO₂ emissions, such as energy efficiency, alternative binders and fuels, and carbon capture [5]. However, more than 50% of the OPC emissions are related to the decomposition of limestone (CaCO₃) into lime (CaO) and CO₂ [6]. Thus, the development of low-carbon binders is increasingly gaining attention. One of the promising binders are alkali-activated materials (AAMs), which include also the so-called geopolymers that are based on low-calcium precursors. AAMs are synthesized from either aluminosilicate or calcium aluminosilicate precursors in highly alkaline conditions [7]. The most common precursors are metakaolin, coal fly ash, and ground granulated blast furnace slag (GGBFS). Metakaolin derives from the calcination of naturally occurring kaolin clay at around 750 °C, while coal fly ash and GGBFS are by-products of the energy and steel production industries, respectively [3]. It has to be noted that the availability of the latter precursors is expected to decrease in the following years due to green transition changes taking place in the energy and steel production sectors [4]. However, GGBFS is a well-known AAMs precursor, and thus, it will be considered as a model system in the present study.

Alkali activation of metakaolin and class F fly ash (low-calcium) leads mainly to a reaction product known as sodium-aluminum-silicate-hydrate (N-A-S-H) gel. In contrast, when GGBFS and class C fly ash (high calcium) react with the alkalis, the reaction product primarily formed is calcium-aluminum-silicate-hydrate (C-A-S-H) gel [7, 8], often accompanied by Mg–Al and Ca–Al layered double hydroxides as secondary reaction products [9].

Thereafter, two main pathways are used for the synthesis of AAMs [6, 10]: two-part and one-part mix. Most of the current research and applications of AAMs are produced by a two-part mix, which is comprised by the reaction of a concentrated alkali aqueous solution and a solid precursor. However, their large-scale utilization can be limited by the handling of the alkali solutions. Meanwhile, one-part mix is formed by mixing dry-form alkali activators with the solid precursor and water. The precursor and solid activator can be ground separately and combined after, or they can be co-ground. The one-part approach has been seen to lower the mechanical performance; however, it has gained attention in the last decade from both

academia and industrial sectors as it provides safer and easier-to-handle approach for cast-in-situ applications, for instance, than the two-part approach [10]. Nevertheless, it should be noted that the very first publications on AAMs more than 120 years ago were based on the one-part approach [11, 12].

Even though there is a significant amount of research published on the mechanical properties and different mix design options of one-part synthesis [13–16], there is a lack of documentation on the difference between one- and two-part alkali-activated binders using identical mix designs in terms of molar ratios of SiO₂, Al₂O₃, and Na₂O in both cases. A recent study from Ren et al. [10] compared one-part and two-part synthesis of alkali-activated GGBFS mortars with a water-to-solids ratio of 0.4 and using anhydrous metasilicate as solid activator. They observed an increase of temperature during the mixing procedure and a slower setting time for one-part when compared to two-part. However, the obtained materials exhibited similar workability and reached compressive strengths after 28 days of 60 MPa as one-part, and 67 MPa as two-part [10]. A prior study from Nematollahi et al. [17] synthesized one-part mixes using a mixture of class F fly ash, GGBFS, calcium hydroxide with different grades of sodium hydroxides and sodium silicates as the alkali activators. Thereafter, a conventional two-part alkali-activated mix with the commonly used activator solution was made for comparison. The highest compressive strength reached at 28 days was 37 MPa for a heat cured one-part mix, and it was 5 MPa lower than the two-part reference mix. No other studies have been found in the literature comparing systematically one-part and two-part synthesis using similar mix proportions, and both of them investigated only high-calcium precursors. Prior comparisons of one-part and two-part synthesis in low-calcium systems such as metakaolin have not been previously published.

Thus, the aim of this study is to investigate and compare fresh and hardened state properties, reaction kinetics and phase evolution of alkali-activated metakaolin and GGBFS paste when prepared as one-part and as two-part. The aim is to understand how the properties are influenced by the production method in the case of low- and high- calcium systems (i.e., using metakaolin and GGBFS, respectively).

Materials and Methods

Raw Materials

Metakaolin (MetaMax) was supplied by BASF Chemicals (Ludwigshafen, Germany) and GGBFS was provided by Finnsementti (Raahe, Finland). The median particle sizes (D₅₀) of metakaolin and GGBFS were around 4.6 and 9.4 μm, respectively. The chemical oxide composition of

Table 1 Chemical oxide composition of BASF's metakaolin and Finnsementti's GGBFS

Chemical oxide composition of metakaolin (wt%)										
SiO ₂	Al ₂ O ₃	Na ₂ O	K ₂ O	TiO ₂	Fe ₂ O ₃	CaO	MgO	P ₂ O ₅	SO ₃	LOI
53.0%	43.8%	0.23%	0.19%	1.70%	0.43%	0.02%	0.03%	0.03%	0.03%	0.46%
Chemical oxide composition of GGBFS (wt%)										
CaO	SiO ₂	Al ₂ O ₃	Na ₂ O	K ₂ O	TiO ₂	Fe ₂ O ₃	MgO	P ₂ O ₅	SO ₃	LOI
38.51%	32.33%	9.58%	0.51%	0.53%	1.70%	1.23%	10.24%	0.01%	4%	0.00%

each precursor is shown in Table 1. SiO₂ and Al₂O₃ are the main components of metakaolin, with contents of 53.0 wt% and 43.8 wt%, respectively. Meanwhile, the main components of GGBFS are CaO and SiO₂, with contents of 38.51 wt% and 32.33 wt%, respectively. In addition, other minerals have also significant percentages such as 10.24 wt% MgO and 9.58 wt% Al₂O₃.

The employed alkali activators, sodium hydroxide (NaOH) reagent grade powder with a 97% purity and anhydrous sodium metasilicate (Na₂SiO₃) powder with 50–53% SiO₂ and 50–47% Na₂O, were purchased from Sigma Aldrich.

Sample Preparation

The sample preparation of two-part AAMs mixes consisted of preparing in advance the alkali solutions. The NaOH is dissolved in half the total amount of distilled water and the Na₂SiO₃ in the other half. Each solution are then left to cool down to room, temperature for 2 h, while continuous stirring. Thereafter, the solid precursor and the solutions of NaOH and Na₂SiO₃ were mixed in a Hobart mixer at high speed for 4 min. Once a homogenous mixture was obtained, the properties of the paste were ready to be tested.

Meanwhile, the sample preparation for one-part AAMs mixes consisted of mixing the dry activators (NaOH and Na₂SiO₃) with the solid precursor in a Hobart mixer for 2 min at low speed. Then, distilled water was added to the bowl and mixing was continued at high speed for another 4 min.

As aforementioned, a metakaolin and a GGBFS AAMs system have been studied when produced as one-part and as two-part. A mix formulation has been selected for each precursor based on previously reported optimum molar oxide

ratios (such as SiO₂/Al₂O₃ = 1.8–3.0 for metakaolin, and 3.0–6.0 for GGBFS) [18, 19], while ensuring the workability of the pastes (Appendix S1). Table 2 shows the mix designs for the metakaolin and the GGBFS alkali-activated pastes. The water-to-solids (*w/s*) ratio of the metakaolin paste was set quite high when compared to the previously reported optimal values (*w/s* = 0.4–0.5) [19, 20], due to the poor workability of one-part metakaolin at lower water contents. Other studies [21] have also reported metakaolin alkali-activated binders using *w/s* of 0.8. The high water demand of one-part alkali-activated paste could be a combination of the higher mixing temperature originated from the dissolution of the solid alkali activators, the low-packing density of metakaolin particles, and their shape, which results in an increased water absorption (Blaine fineness of metakaolin is around 19,000 m²/kg) [22].

Meanwhile, in the mix design for the GGBFS alkali-activated paste, the SiO₂/Al₂O₃ is set higher than for alkali-activated metakaolin, as GGBFS contains less Al₂O₃. On the other hand, the water-to-solids ratio can be much lower, as GGBFS has a higher density of particles and lower Blaine fineness (400 m²/kg) than metakaolin [22].

Test Procedures

Setting Time and Isothermal Calorimetry

The setting time was tested using an automatic Vicat apparatus with continuous penetration at ambient conditions (E044-03N), following the EN196-3 standard [23]. Isothermal calorimetry experiments were then conducted using a TAM Air isothermal calorimeter at a base temperature of 22 °C. The fresh pastes were weighed into an ampoule and immediately placed in the calorimeter to record heat flow.

Table 2 Mix design for one- and two-part metakaolin and GGBFS alkali-activated paste

Metakaolin (g)	GGBFS (g)	Sodium hydroxide (g)	Solid sodium silicate (g)	Water (g)	SiO ₂ /Al ₂ O ₃ (mol/mol)	Na ₂ O/SiO ₂ (mol/mol)	<i>w/s</i> (g/g)
400	0	22	46	325	2.3	0.2	0.69
0	400	12	28	165	6.3	0.2	0.40

All results were normalized by the total mass of the paste. An equal amount of water as present in the paste samples was used as a reference sample for each measurement. The calorimetric data were recorded for a period of 72 h. The heat release rate and total reaction heat were normalized by the total mass of precursors.

Mass Loss, Shrinkage, Density, and Mechanical Strength

The fresh homogenous mixtures were cast into 40 mm cubes and placed for 30 s on a vibration table to remove any trapped air bubbles. The samples were then inserted in a curing chamber at $21\text{ }^{\circ}\text{C} \pm 2\text{ }^{\circ}\text{C}$ and 80% relative humidity (RH). They were unmoulded after 24 h, and they were left in the curing chamber until testing. The mass loss, shrinkage, and density were measured after 1, 3, 7, 14, 21, and 28 days. The shrinkage was determined by measuring the change in length of 40 mm cubes using a micrometer with 0.01 mm accuracy. The length change (LC) was then calculated as $LC = \frac{40-L_i}{40} \times 100$, where L_i is the length at each tested day. The weight of each cube was recorded before each length measurement. The density (ρ) was then back-calculated, knowing the volume (V) of the sample and the weight (m), $\rho = \frac{m}{V}$. Compressive strength tests were performed on the 40 mm cubic samples using a Digitec E160-01D compression machine with a constant loading rate of 0.750 MPa/s. Tests were performed after 3, 7, and 28 days. Each reported value “Mass Loss, Shrinkage and Density” and “Compressive Strength” corresponds to the average of six measurements (standard deviation has been illustrated).

Thermal, Morphological, Elemental, and Mineralogical Analysis

The formulations were further characterized by thermogravimetric analysis/differential scanning calorimetry (TGA/DSC), scanning electron microscopy (SEM), energy-dispersive X-ray spectroscopy (EDS), X-ray diffraction (XRD), and solid-state magic angle spinning nuclear magnetic resonance (MAS NMR). The wet alkali-activated pastes were cast in 10 mm cubes, vibrated for 30 s and placed in the curing chamber ($21\text{ }^{\circ}\text{C} \pm 2\text{ }^{\circ}\text{C}$ and 80% RH) until testing. The samples had to be powdered in a ball mill at 350 rpm for 3 min before testing them on TGA–DSC, XRD, and MAS NMR, while hardened dry cubes were used in SEM–EDS.

TGA/DSC was used to measure the thermal stability and phase composition when exposed at high temperatures of the different formulations at 28 days. The analyses were performed using a Netzsch STA 449 in the temperature range between 0 and 1100 $^{\circ}\text{C}$, with a heating rate of 10 $^{\circ}\text{C}/\text{min}$ and with an atmosphere of 10% O_2 and 90% N_2 .

The morphological and elemental composition were studied after 28 days by SEM–EDS. A Thermo Scientific Prisma

E with a 20 kV acceleration voltage was used. The samples were non-polished to study the morphology with secondary electron images and they were embedded in epoxy and then polished for EDS analysis.

Thereafter, the mineralogical and phase composition of the raw materials and the alkali-activated samples were investigated at 28 days by using a Huber G670 X-ray powder diffractometer with $\text{CuK}\alpha$ ($\lambda = 0.154\text{ nm}$). The scans were performed within the range of $2\theta = 5^{\circ}$ – 100° at 40 kV and scanning times of 10 min. Phase identification was done by the MATCH database.

Finally, the solid-state MAS NMR experiments were performed at 1 and 28 days, with the help of a Bruker Avance III 300 spectrometer. The samples were introduced to 7 mm zirconia rotors and the spinning frequency employed was 7 kHz. The frequency of the ^{27}Al experiments was 78.24 MHz, and 2048 scans were collected with a repetition time of 2 s. The excitation pulse length and angle were 1.0 μs and 30° , respectively. Chemical shift referencing was performed using $\text{Al}(\text{NO}_3)_3$ as an external standard. In case of ^{29}Si experiments, the frequency was 59.65 MHz. During the experiment, 8192 scans were collected with a repetition time of 3 s. The excitation pulse length and angle were 5.5 μs and 90° , respectively. For chemical shift referencing, tetramethylsilane was used as an external standard.

Results and Discussion

Setting Times

The initial and final setting times were measured for each alkali-activated system to investigate the effect of two-part and one-part on the stiffening of the paste. The initial setting indicates the time that the paste starts to gain consistency, while the final setting indicates the time that the paste has completely stiffen and can sustain some load. This means that the initial setting time provides the time frame that the alkali-activated paste is workable and that can be casted/shaped. The EN 196-3 [23] prescribes that the initial setting time of a cement paste should not be shorter than 45 min and the final setting should not be longer than 10 h. Table 3

Table 3 Initial and final setting time of the different alkali-activated formulations

Sample	Initial setting time (min)	Final setting time (min)
GGBFS two-part	73 ± 3	135 ± 3
GGBFS one-part	119 ± 2	226 ± 6
MK two-part	47 ± 1	105 ± 2
MK one-part	74 ± 5	121 ± 4

shows the setting time results obtained for the different pastes, as an average of 3 samples including the standard deviation. It can be observed that all samples comply with the standards.

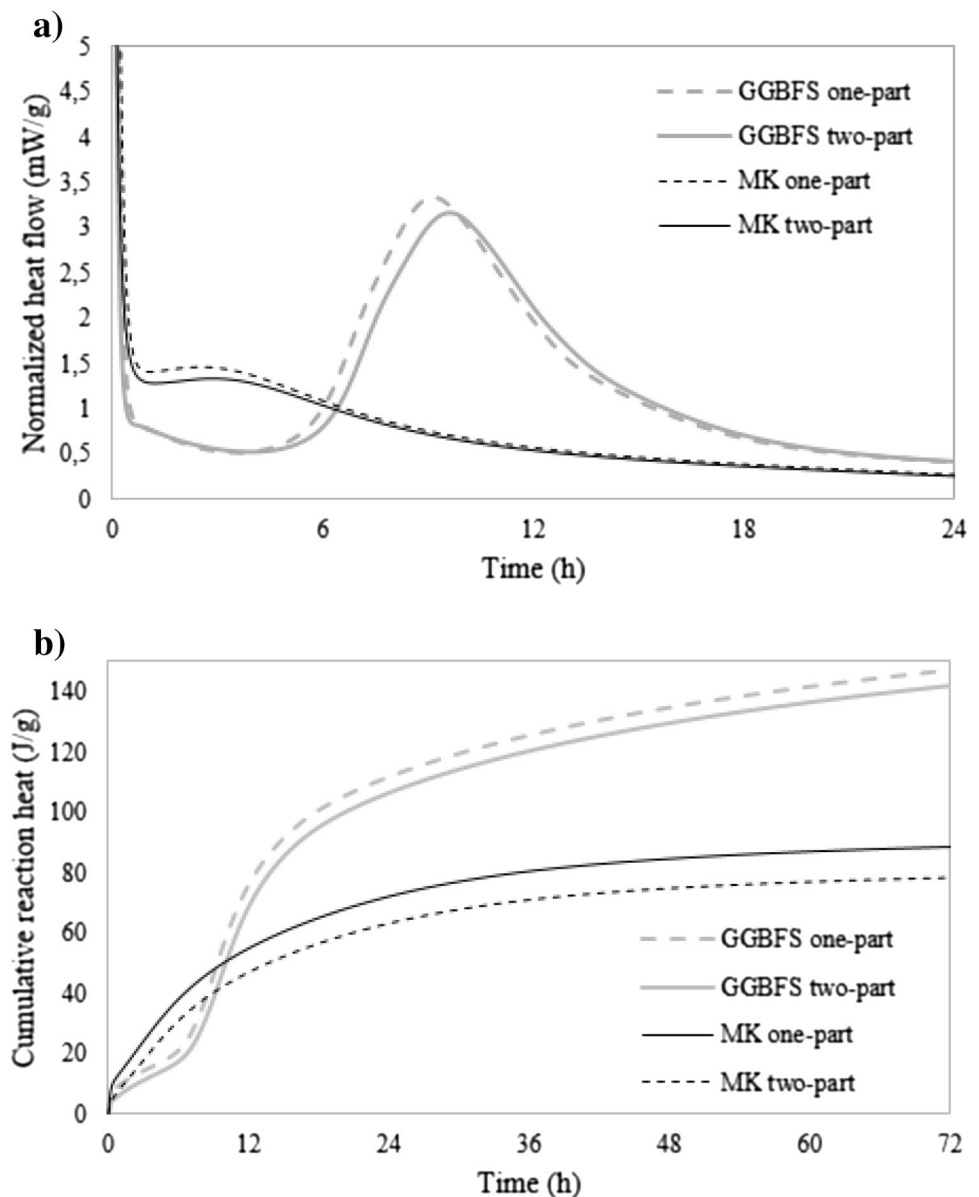
Despite one-part and two-part systems having the same mix design, a clear difference in setting times can be observed. One-part mixtures have a slower initial and final setting time with respect to two-part mixtures. One-part GGBFS has a 67% slower final setting time when compared to two-part, and one-part metakaolin has a delay of 15% when compared to two-part. This could be due to the fact that the alkali activator powders were mixed with the dry precursors before they were dissolved in water, thus this delayed the dissolution of the precursors, as well as the following gelation and condensation reactions. This slower

hardening rate for one-part alkali-activated binder in comparison with similar two-part system has also been observed by [10] and [24]. Another observation is that metakaolin binders set faster than GGBFS binders. This could be explained by the higher water absorption of metakaolin and the higher content of NaOH in the mix design.

Isothermal Calorimetry

The normalized heat flow and cumulative normalized heat of the one-part and two-part alkali-activated pastes are shown in Fig. 1 (Appendix S2). For each heat flow curve (Fig. 1a), there is a first exothermic peak that arises in the first half an hour after the test started. This peak is termed as the pre-induction period and is attributed to the wetting and

Fig. 1 **a** Normalized heat flow (mW/g) and **b** cumulative reaction heat (J/g)



chemical dissolution of the solid precursors [21, 25]. This initial dissolution peak is then followed by a peak valley or dormant period, which has a lower heat release rate, and is known as the induction period. Subsequently, a second exothermic peak is observed [21, 26]. This peak is generally associated with the nucleation, growth, and precipitation of the reaction products [21, 27]. From the heat flow curves, it can be seen that there is no difference in the reaction kinetics between one-part and two-part systems, when using the same precursor in both. However, one-part seems to display a shorter induction period. This is probably due to the faster precipitation of certain reaction products under a raised mixing temperature due to the dissolution of the solid alkalis, observation that corresponds well with other literature [10, 28, 29].

The alkali-activated metakaolin binder presents a dormant period with a high heat release but for an extremely short period and then it has a broadened second peak. In fact, the induction period can be barely detected because of the overlapping between the initial and acceleration peak stages. Previously reported work [21] showed similar heat flow curves, and they observed that the higher the activator concentration the larger the broadening of the second peak. Conversely, the alkali-activated GGBFS binder has an induction period with a lower heat release and at around 10 h, the second peak arises reaching higher heat flows than for the metakaolin system. According to prior studies [21], the induction period increases its magnitude at higher alkali concentration. In addition, the heat flow reaction process in GGBFS is similar to what is observed in the cement hydration process [21, 25].

The cumulative heat release of the different alkali activated binders at 72 h can be seen in Fig. 1b. The cumulative heat increases rapidly up to 48 h, thereafter the growth in the cumulative curves is much slower. The GGBFS cumulative heat curve is higher than for the metakaolin paste, and one-part mix seems to lead to a higher cumulative reaction heat for both precursors, being a 3.6% increase for one-part GGBFS and 11.5% higher for metakaolin one-part system. However, it can be observed that metakaolin pastes have a higher heat of reaction than GGBFS pastes for the first 6 h of reaction. This could also be correlated with their faster setting time observed in Table 3.

Mass Loss, Shrinkage, and Density

The mass loss, shrinkage and density of the synthesized alkali-activated binders were tested over a period of 28 days. Those parameters are largely influenced by the porosity, composition, and curing conditions of the specimens [30]. Generally, the decrease of sample weight during the curing process of AAMs is caused by the evaporation of moisture from the pores. Water tends to be first removed from larger

pores (macropores) and then from smaller pores (meso- and micropores) during the drying process. After the water has evaporated from the macropores, water in the mesoscale pores tends to evaporate, which can then generate large capillary stresses that increase the shrinkage of the pastes [31].

The results of mass loss are presented in Fig. 2. It can be seen that alkali-activated metakaolin mixes have an abrupt mass loss during the first 7 days, and then they stabilize. This is probably due to the evaporation of water from the macropores which tends to be rapid on the early ages of curing. Moreover, one-part metakaolin seems to lower the mass loss when compared to two-part. This could be related with a lower content of macropores and lower moisture evaporation. Regarding alkali-activated GGBFS pastes, they do not appear to have a change in weight over time nor difference between one-part or two-part mix. This could be explained by the lower water-to-solids ratio and by a better compaction of the fresh alkali-activated GGBFS, which minimizes the presence of macropores.

Thereafter, Fig. 3 illustrates the uniaxial length change of all the pastes in the course of 28 days of curing. From these results, it is observed that the uniaxial length change of all the specimens was more pronounced during the first 21 days. Alkali-activated metakaolin binder seems to have a lower shrinkage when compared to GGBFS, and only a 0.16% length difference between one- and two-part was observed at 28 days. The shrinkage in metakaolin binders is probably related to evaporated water and from an inadequate compaction of unreacted metakaolin particles in the slurry system during the early ages. Meanwhile, GGBFS two-part seems to have a higher shrinkage, as it has a 0.58% length difference with GGBFS one-part at 28 days. Shrinkage in GGBFS seems to be greatly influenced by the internal capillary stress generated due to the loss of water in the mesoscale pores. This is supported by the fact that no major mass loss was

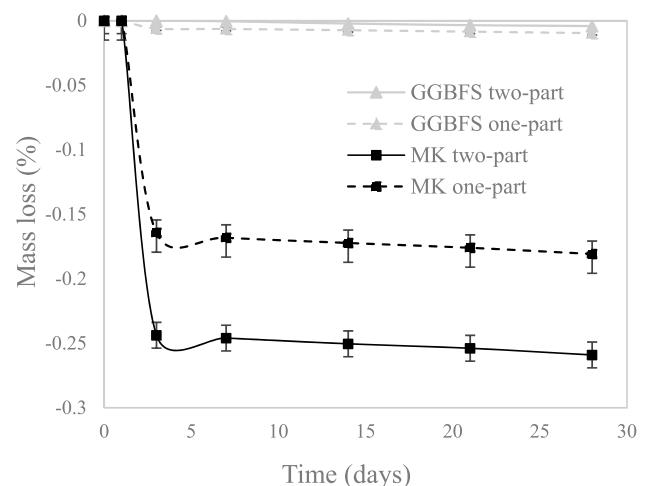


Fig. 2 Mass loss (%) of the specimens for a period of 28 days

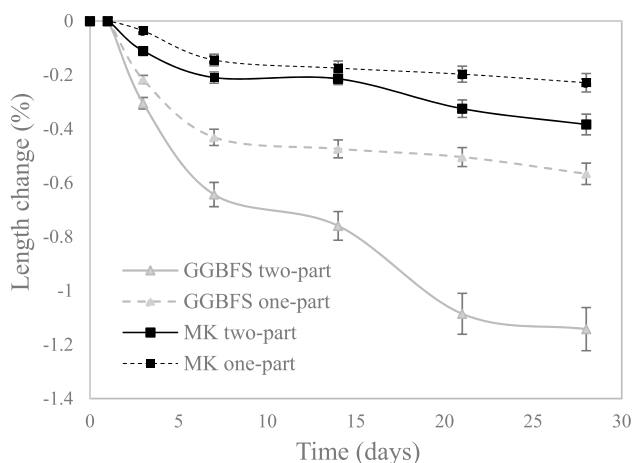


Fig. 3 Uniaxial length change (%) of the specimens for a period of 28 days

observed. Thus, the total content of lost water is lower in alkali-activated GGBFS than in metakaolin, but the capillary stress of the mesopores is higher and it results in an increased length change. This means that the alkali-activated GGBFS undergoes an autogenous shrinkage, in which the water is consumed by the reaction products, whereas the alkali-activated metakaolin undergoes mostly drying shrinkage due to water evaporation.

In addition, the ambient curing conditions of the pastes could be greatly affecting the shrinkage, especially for alkali-activated GGBFS. Other studies [31] have determined that higher curing temperatures can accelerate the reaction process, reduce the unreacted precursor, and decrease the shrinkage of the paste.

The density was calculated after a curing period of 28 days. The average density of alkali-activated GGBFS was higher than for metakaolin. Comparing the average density of metakaolin (1.6 g/cm^3) and GGBFS paste (2.1 g/cm^3) after 28 days with a Portland cement paste (2.3 g/cm^3), it can be seen that the metakaolin pastes have a lower density. This is mainly due to the higher porosity of metakaolin pastes and the low-packing density of metakaolin when compared to GGBFS or Portland cement. No differences were observed between one-part mix and two-part mix.

Compressive Strength

The average compressive strength development tested at 3, 7, and 28 days for the different alkali-activated mixes is shown in Fig. 4. From the figure, it is seen that at 7 days, all the specimens have gained 80 to 90% of the compressive strength obtained at 28 days. It can also be observed that alkali-activated GGBFS reaches strengths above the 32.5 strength class prescribed in the EN197-1 standard [32], whereas alkali-activated metakaolin has lower strengths

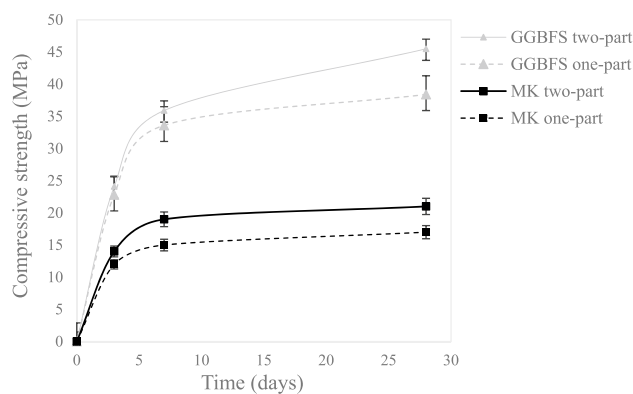


Fig. 4 Compressive strength development of the specimens

than the required by EN standards. Nevertheless, it has to be noted that the EN standard is based on mortars and concretes and it has been reported that the compressive strength of cement pastes increases 30–35% when fine and coarse aggregates are added [33]. Thereafter, one-part and two-part mixes present similar strength development up to 3 days of curing in both systems, and then two-part mix seems to reach higher compressive strengths. At 28 days of curing, one-part metakaolin is about 82% the strength of two-part and one-part GGBFS is 85% the strength of two-part.

The similar compressive strength development between one-part and two-part could be explained by considering that one-part mix has counteracting effects. On the one hand, the dissolution of the precursor into the alkaline activator is delayed, to which some extent hinders the nucleation, growth, and precipitation of reaction products. On the other hand, there is a significantly increased temperature due to the contact of sodium metasilicate powder with water, which increases the heat of reaction and partially improves the solubility and diffusivity [34].

Another observation is that the alkali-activated GGBFS leads to a higher average compressive strength at 28 days (45.5 MPa two-part and 38.4 MPa one-part) when compared to metakaolin pastes (21.1 MPa two-part and 17.2 MPa one-part). This could be explained by the lower porosity and denser microstructure that GGBFS pastes exhibit. Moreover, the reduced compressive strength of alkali-activated metakaolin with respect to GGBFS might be associated with the higher water demand, higher water evaporation, and some internal defects caused by the rapid formation of hard shells around the unreacted metakaolin particles because of the increased heat of reaction in the first hours after mixing. Moreover, a study [35] suggests that the addition of solid NaOH in one-part GGBFS systems, dissolves solid sodium silicate (with high $\text{SiO}_2/\text{Na}_2\text{O}$ ratio), newly formed aluminosilicate gels and the precursor. This means a decrease of compressive strength in the one-part GGBFS systems when solid sodium silicate activators with a low $\text{SiO}_2/\text{Na}_2\text{O}$

ratio are used. This is in agreement with the slower setting time observed in Table 3, and with their lower compressive strength when compared to two-part (Fig. 4).

Thermal Analysis (TGA/DSC)

The TGA–DSC analysis was performed for all the alkali-activated formulations investigated (Appendix S3). In Fig. 5, the TGA–DSC curves of the alkali-activated metakaolin (one-part and two-part) are shown, and they are compared to the TGA curve of the precursor metakaolin before alkali activation. The first observation from the TGA curves is that there is a mass loss of 10% up to 200 °C for both alkali-activated mixes. Accordingly, an endothermic peak is visible in their DSC curves. This is in agreement with the literature that associates this mass loss with loss of free water or slightly bound water in the alkali-activated metakaolin structure [36]. Thereafter, a further mass reduction of about 2% is observed between 200 and 600 °C. This is attributed to chemical bound water that could result from the condensation of silanol and aluminol groups [36, 37]. The metakaolin before being alkali-activated seems to be thermally stable when heated up to 1000 °C, and no phase changes are observed.

In Fig. 6, the TGA–DSC curves of the alkali-activated GGBFS and the TGA curve of the precursor GGBFS can

be seen. For both one-part and two-part, there is a great mass loss up to 300 °C of 16 and 14%, respectively. This mass loss is associated with loss of free bound water from the calcium aluminosilicate hydrate (C–A–S–H) gel and is supported by a high intensity endothermic peak in the DSC curve. Subsequently, there is another 4% mass loss between 300 and 720 °C in each alkali-activated mix. This is attributed to the loss of chemically bound water and dehydroxylation of hydrotalcite-like phases [10, 13]. Thereafter, between 720 and 760 °C, a further 1% mass loss is observed and is probably due to the decomposition of calcium hydrates and decarbonation of calcite. This is also attributed to an endothermic phase in their DSC curves. An exothermic peak can also be seen around 1000 °C and that could be associated with some crystalline phase formation. The TGA curve of precursor GGBFS shows that it is also thermally stable up to 1000 °C, as it was observed for metakaolin. However, the influence of alkali activation in each precursor is different. The mass loss due to high temperature exposure is more pronounced for alkali-activated GGBFS binders (with approximately 20% mass loss) than for alkali-activated metakaolin binders (with a 12% mass loss).

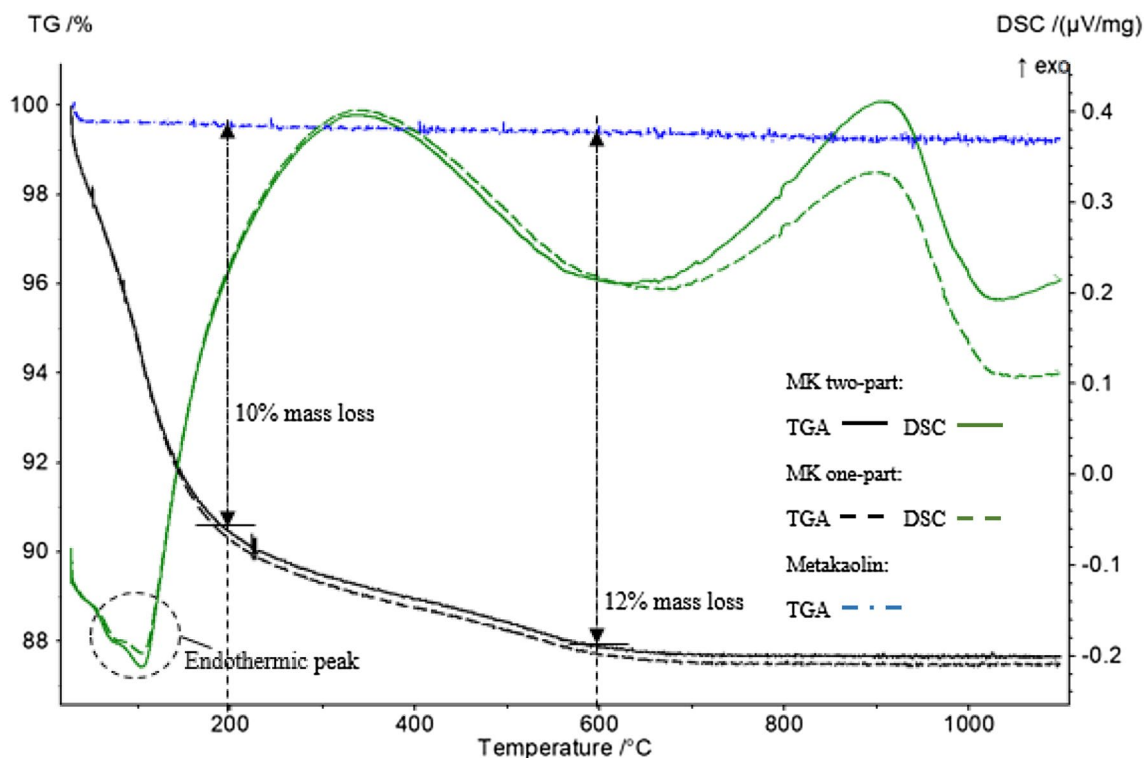


Fig. 5 TGA–DSC of the precursor metakaolin, alkali-activated one- and two-part metakaolin at 28 days

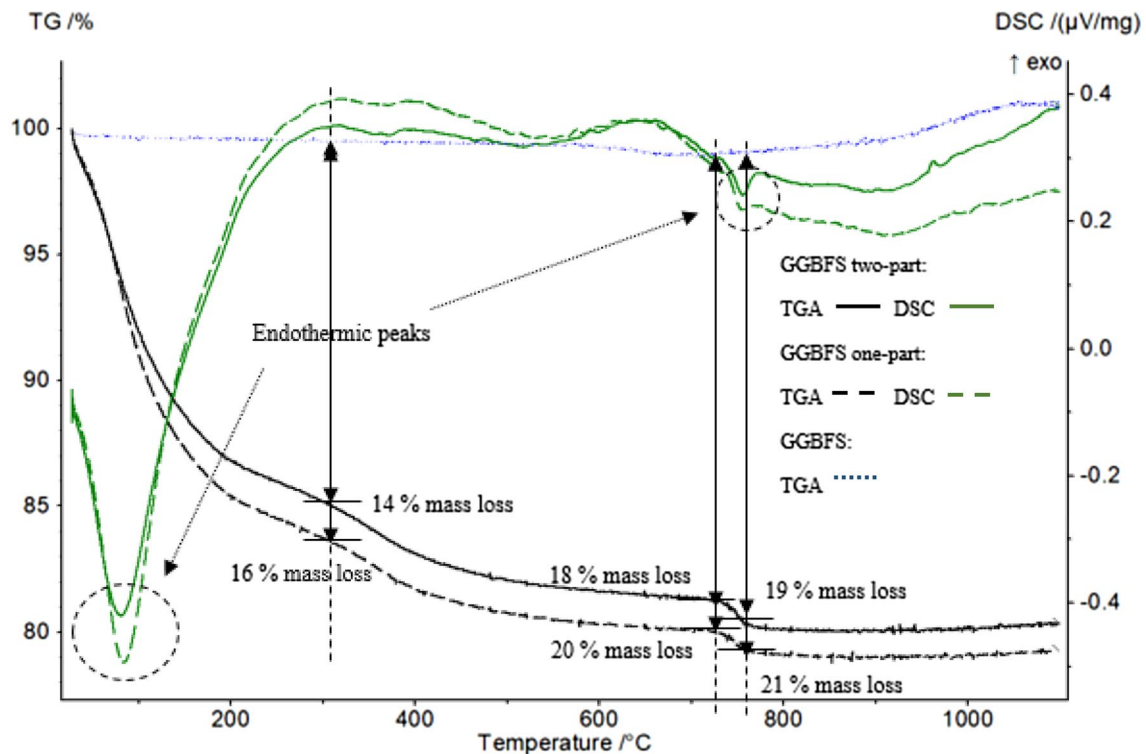


Fig. 6 TGA–DSC of the precursor, alkali-activated one- and two-part GGBFS at 28 days

SEM–EDS Analysis

The morphological analysis performed by SEM on the surfaces of both alkali-activated metakaolin and GGBFS is shown in Fig. 7. In Fig. 7a, b, it can be observed that one- and two-part metakaolins are characterized by having amorphous particles with rough and uneven edges. The more layered, needle-like, or plate-like particulates have been previously related to unreacted metakaolin [38]. It can also be seen that the matrix is not a homogenous blend of well-dissolved particulates, instead is the combination of amorphous and needle-like particulates embedded in a matrix. This greatly affects the compressive strength and durability of the alkali-activated metakaolin pastes [38]. In Fig. 7c, d, the secondary electron images for one-part and two-part GGBFS show that the matrix presents some micro-cracks, pores, and particulates. Other studies have associated those particulates as unreacted slag grains or anhydrous slag grains [39, 40].

Thereafter, an EDS analysis of each specimen has been performed to analyze the elemental composition of polished samples (Appendix S4). Point analysis has been the method used to analyze the composition of the matrix, and an average of 3 points have been performed per sample. Table 4 compares the EDS analysis of the two-part and one-part alkali-activated metakaolin paste. Both pastes are mainly composed by silica (Si), aluminum (Al), oxygen (O), and sodium (Na). However, it can be seen that two-part mix

presents higher content of dissolved Si and Al (%) with respect to one-part. This could be indicating an increased formation of N–A–S–H gel. Meanwhile, Table 5 compares the EDS analysis of two-part and one-part GGBFS, showing that they are both constituted primarily by calcium (Ca), silica (Si), aluminum (Al), oxygen (O), sodium (Na), and magnesium (Mg). Similarly as with the metakaolin system, two-part GGBFS shows a slightly higher content of Ca, Si, and Al (%) than one-part, which could be explained by a higher formation of C–A–S–H gel.

XRD Analysis

The X-ray diffraction patterns of the two alkali-activated systems are shown in Figs. 8 and 9. The alkali-activated one- and two-part metakaolin present the amorphous broad peak characteristic from metakaolin; however, it can be observed that the center of the broad band is shifted to larger 2θ angles. This indicates that the metakaolin amorphous phase has been dissolved and a new phase has formed [41]. Some studies have associated this peak with the presence of N–A–S–H gel, and the size of it depends on the amount of gel produced [42, 43]. From the phase analysis, quartz (Pdf number: 010-80-2147) has been identified in both the alkali-activated metakaolin and in the precursor. Nevertheless, another crystalline phase, aluminum oxide, has been identified in the two-part metakaolin (Pdf number: 010-78-5519).

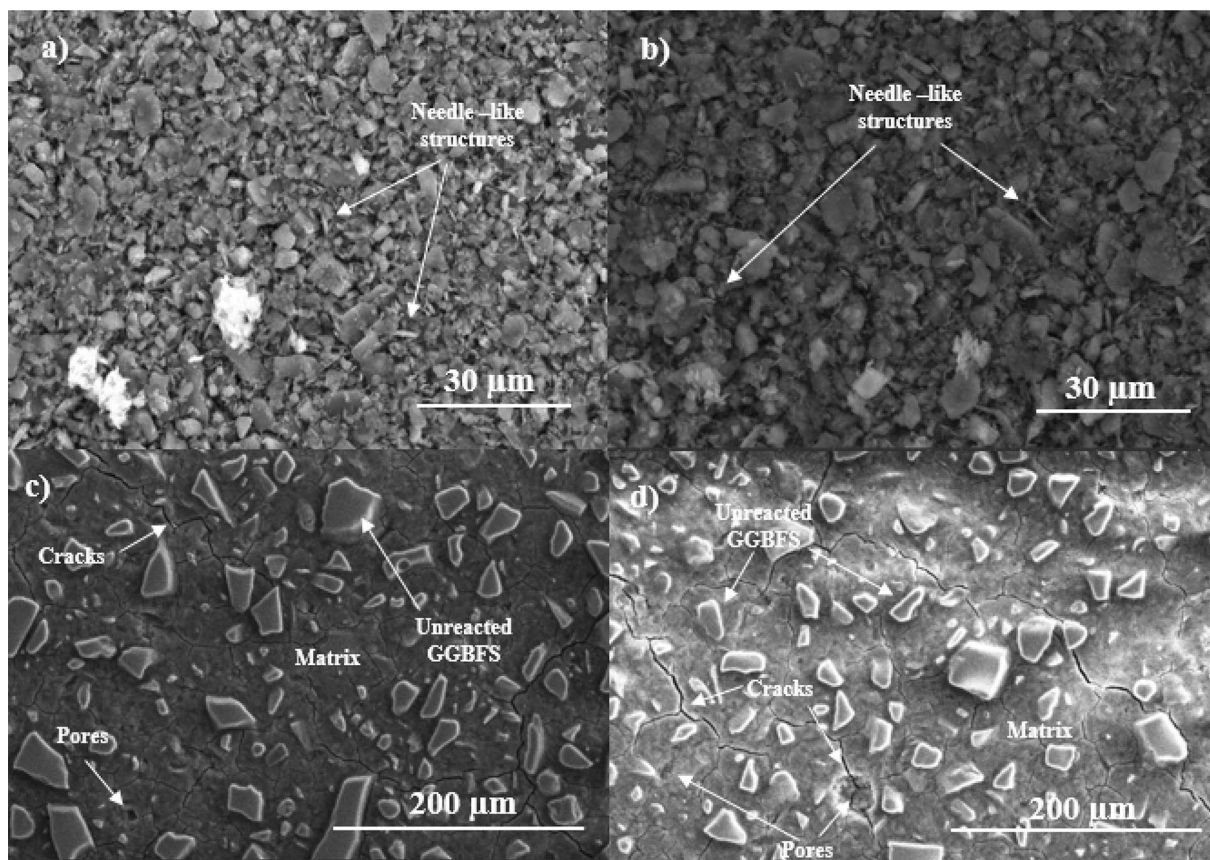


Fig. 7 Secondary electron images showing the surface morphology of **a** alkali-activated metakaolin one-part and **b** two-part at 20 kV and $\times 2000$; and **c** alkali-activated GGBFS one-part and **d** two-part at 20 kV and $\times 500$

Table 4 EDS analysis of 28 day cured polished two-part and one-part metakaolin paste at 20 kV and 500x

Element	Two-part metakaolin		One-part metakaolin	
	Spectrum weight (%)	Spectrum atom (%)	Spectrum weight (%)	Spectrum atom (%)
O	33.58	46.14	43.31	57.94
Si	31.09	24.33	24.27	17.68
Na	6.34	6.07	7.04	6.26
Al	26.00	21.19	20.93	15.87
Others	2.99	2.27	4.45	2.25

Regarding alkali-activated one- and two-part GGBFS, an amorphous hump is also observed, which is also present in the precursor GGBFS. From the XRD patterns, it can be seen that GGBFS precursor is mainly composed of amorphous phases, and one- and two-part have a sharper peak at $30^\circ 2\theta$ than for GGBFS, which is generally attributed to C-(N)-A-S-H gel [9, 25]. For

Table 5 EDS analysis of 28 day cured polished two-part and one-part GGBFS at 20 kV and $\times 500$

Element	Two-part GGBFS		One-part GGBFS	
	Spectrum weight (%)	Spectrum atom (%)	Spectrum weight (%)	Spectrum atom (%)
O	39.95	56.23	41.47	57.05
Ca	27.46	15.43	24.08	13.22
Si	18.47	14.81	16.34	12.81
Na	5.73	5.61	7.11	6.81
Al	3.47	3.01	3.57	2.91
Mg	1.84	1.7	3.22	2.92
Others	3.08	3.21	4.21	4.3

the alkali-activated GGBFS, the identified phases have been quartz (Pdf number: 010-80-2147) and Mg–Al–OH hydrotalcite ($Mg_6Al_2(OH)_{18} \cdot 4.5H_2O$, Pdf number: 000-35-0965), which are also in agreement with previous observations [9].

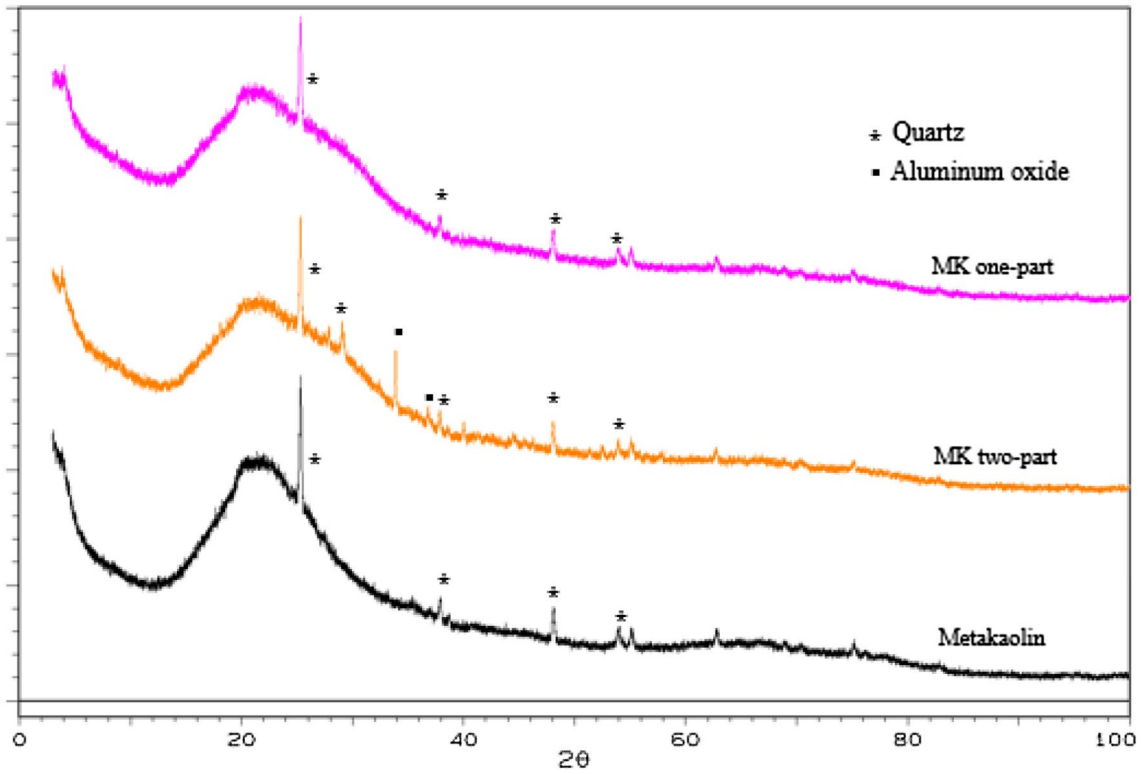


Fig. 8 XRD pattern of raw metakaolin compared to alkali-activated one- and two-part

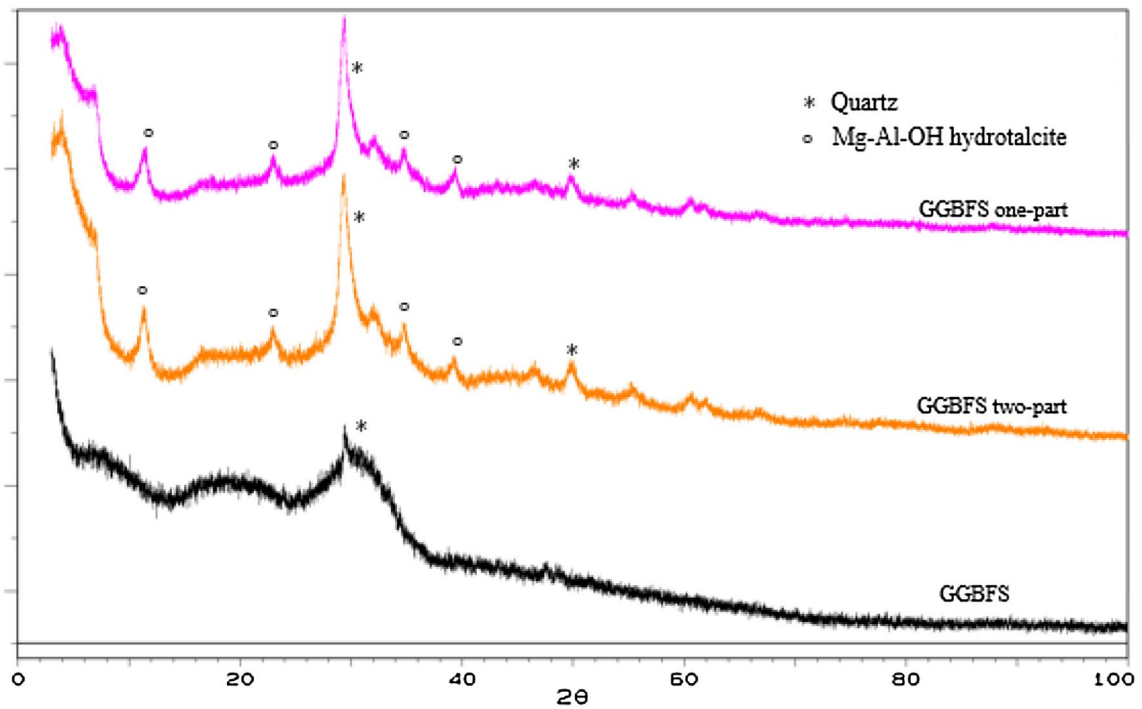


Fig. 9 XRD pattern of raw GGBFS compared to alkali-activated one- and two-part

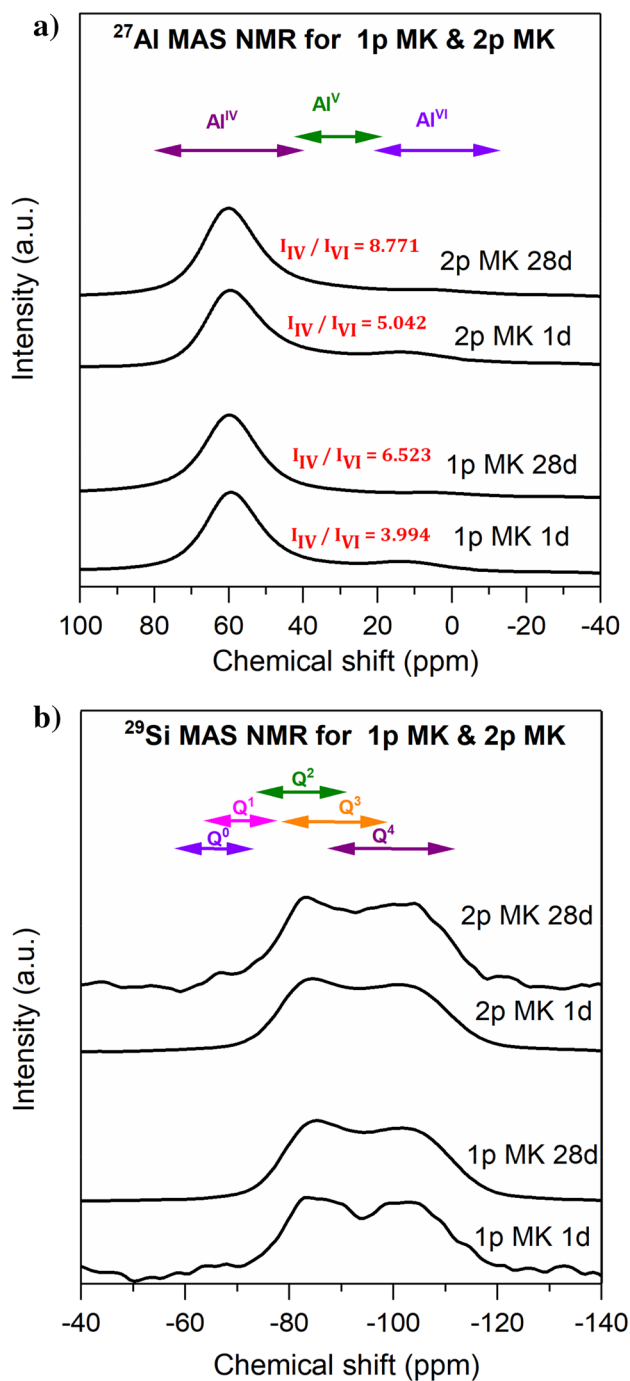


Fig. 10 a ^{27}Al MAS NMR and b ^{29}Si MAS NMR of one-part and two-part metakaolin-based AAMs

Solid-State MAS NMR

The results of the ^{27}Al MAS NMR analysis of the one-part and two-part metakaolin-based AAMs are shown in Fig. 10a. The one-part metakaolin-based sample after 1 day (1p MK 1d) has a strong tetrahedral signal centered around 60 ppm, which corresponds to the tetrahedral aluminum present in

the N–A–S–H gel [44]. This is in agreement with XRD analysis which indicated the presence of N–A–S–H gel in the same sample. The sample 1p MK 1d also shows a weak octahedral signal spanning from 0 to 20 ppm. This signal belongs to the unreacted metakaolin [44]. The ratio ($I_{\text{IV}}/I_{\text{VI}}$) of intensity of the tetrahedral signal (which corresponds to product phase) to that of the octahedral signal (which corresponds to the reactant) could be used to represent the extent of reaction. $I_{\text{IV}}/I_{\text{VI}}$ for 1p MK 1d is around 3.994. The sample 1p MK 28d also shows the prominent tetrahedral signal around 60 ppm. $I_{\text{IV}}/I_{\text{VI}}$ for this sample is 6.523, which is higher than the corresponding value for 1p MK 1d, thereby indicating the progress of the reaction as the sample is cured from 1 to 28 day. The two-part metakaolin-based AAMs (2p MK 1d & 2p MK 28d) shows similar trend as has been observed in case of one-part metakaolin-based AAMs (1p MK 1d & 1p MK 28d). Note that $I_{\text{IV}}/I_{\text{VI}}$ for 2p MK 28d is higher than that of 1p MK 28d. This means that extent of reaction in two-part mix is higher than that of one-part mix. This is in agreement with the compressive strength measurement which observed higher strength for the two-part mix when compared to one-part mix after 28 days of curing.

Figure 10b shows the results of the ^{29}Si MAS NMR analysis of the one-part and two-part metakaolin-based AAMs. The sample 1p MK 1d shows two characteristic signals: One signal centered around -102 ppm and another signal centered around -85 ppm. The signal centered around -102 ppm can be attributed to the Q^4 species of the N–A–S–H gel [45]. This is in agreement with the ^{27}Al MAS NMR and XRD analyses which indicated the presence of N–A–S–H gel. The signal around the -85 ppm corresponds to a silicate gel which predominantly consists of Q^2 and Q^3 species. In short, the observations indicate that 1p MK 1d consists of N–A–S–H gel as well as a depolymerized silicate gel richer in Q^3 and Q^2 species. The features observed in case of 1p MK 1d are also found in 1p MK 28d, 2p MK 1d, and 2p MK 28d.

The ^{27}Al MAS NMR analysis of the one-part and two-part GGBFS-based AAMs is shown in Fig. 11a. The one-part mix after 1 day of curing (1p SL 1d) shows two characteristic signals: A tetrahedral signal centered around 70 ppm and an octahedral signal centered around 8 ppm. The signal at 70 ppm could be attributed to two components: (1) tetrahedrally coordinated aluminum incorporated in the C–A–S–H phase and (2) tetrahedrally coordinated aluminum present in the unreacted GGBFS [9]. This is in agreement with the identification of C–A–S–H phase according to XRD analysis. The sharper tetrahedral signal at 8 ppm could be attributed to aluminum present in the hydrotalcite [9, 46], which also has been identified by the XRD analysis. The ratio ($I_{\text{VI}}/I_{\text{IV}}$) of intensity of the octahedral signal to that of the tetrahedral signal could be roughly considered to represent the reactivity of GGBFS. This is due to the following

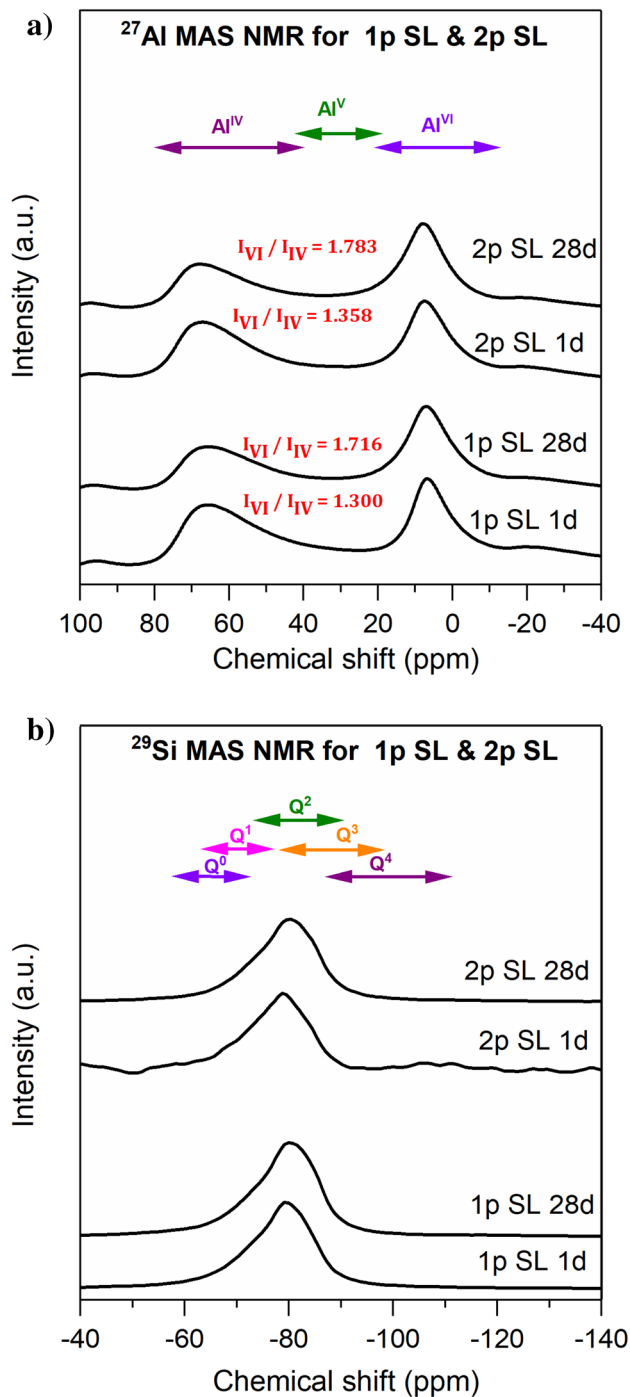


Fig. 11 a ^{27}Al MAS NMR and b ^{29}Si MAS NMR of one-part and two-part GGBFS-based AAMs

reasons: (1) The spectrum of the unreacted GGBFS shows prominent tetrahedral signal, while octahedral signal is considerably less prominent [9]; (2) Reaction of GGBFS leads to emergence of tetrahedral signal corresponding to C–A–S–H phase and octahedral signal corresponding to hydrotoalcite. $I_{\text{IV}}/I_{\text{VI}}$ for 1p SL 1d is 1.300. The sample 1p

SL 28d also exhibits the tetrahedral signal and octahedral signal similar to 1p SL 1d. $I_{\text{IV}}/I_{\text{VI}}$ for 1p SL 28d is 1.716, which is higher than the corresponding value for 1p SL 1d, thereby revealing the progress of the GGBFS reaction as the sample is cured from 1 to 28 day. The two-part GGBFS-based AAMs (2p SL 1d & 2p SL 28d) exhibits similar trend as has been found in case of one-part GGBFS-based AAMs (1p SL 1d & 1p SL 28d). The $I_{\text{IV}}/I_{\text{VI}}$ for 2p SL 28d is higher than that of 1p SL 28d. This means that extent of GGBFS reaction in two-part mix is higher than that of one-part mix. This corroborates the higher compressive strength observed in case of two-part mix when compared to one-part mix after 28 days of curing.

The ^{29}Si MAS NMR analysis of the one-part and two-part GGBFS-based AAMs is shown in Fig. 11b. The sample 1p SL 1d exhibits a signal around -80 ppm. This signal can be attributed to the Q¹, Q², and Q³ species belonging to the C–A–S–H phase whose presence has been also confirmed by XRD and ^{27}Al MAS NMR analysis. This signal is also visible in samples 1p SL 28d, 2p SL 1d, and 2p SL 28d.

Conclusions

Metakaolin and GGBFS were investigated as precursors on the production of one- and two-part alkali-activated binders, using identical mix designs with both preparation methods. From their mix formulations, it was seen that one-part alkali-activated metakaolin demanded having higher water-to-solids ratio than one-part alkali-activated GGBFS. This combined with the fact that the precursors had different compositions, made each system behave differently.

One-part mix was seen to slow the setting time (67% for GGBFS and 15% for metakaolin) and increase the total heat of reaction (3.6% for GGBFS and 11.5% for metakaolin). This was probably due to the delayed dissolution of the precursors and following alkali activation. The evaporation of water during the curing period affected mostly the mass loss of the alkali-activated metakaolin, indicating that they had a larger concentration of macropores. However, the shrinkage of the pastes was larger for GGBFS pastes, meaning that the evaporation of water was occurring at the meso- and microscale pores which created internal capillary stresses and induced shrinkage. Two-part mixes led to the highest compressive strengths of each system. Two-part GGBFS pastes reached an average compressive strength of 45.5 MPa after 28 days, while two-part metakaolin pastes reached an average of 21.1 MPa. The one-part mixes were 85% and 83% of the strength of their respective alkali-activated system, being 38.4 MPa for one-part GGBFS and 17.2 MPa for one-part metakaolin.

The TGA–DSC revealed that alkali-activated metakaolin had a lower mass loss (12%) than alkali-activated GGBFS

(20%) when submitted to high temperatures, for both one-part and two-part mix. Similarly, the morphology of the alkali-activated binders, as obtained by SEM analysis, had no differences between one-part and two-part. However, alkali-activated metakaolin presented a matrix formed of grouped amorphous particulates, while alkali-activated GGBFS seemed to present a more homogenous matrix with some undissolved GGBFS particles. Thereafter, the XRD showed that the alkali-activated metakaolin had the characteristic amorphous peak of metakaolin, and the main crystalline phase identified was quartz. Regarding GGBFS, the XRD patterns showed that GGBFS was mostly amorphous, and that the one- and two-part alkali-activated GGBFS showed the same amorphous broad peak from GGBFS, as well as quartz and Mg–Al–OH hydrotalcite, as crystalline phases. Lastly, the EDS analysis and the solid-state MAS NMR indicated that metakaolin and GGBFS two-part mixes presented more N–A–S–H and C–A–S–H phases, respectively, than in the one-part mix.

Supplementary Information The online version contains supplementary material available at <https://doi.org/10.1007/s40831-022-00606-9>.

Acknowledgements This work was supported by the ProBu project: Process Technology for Sustainable Building Materials Production (Grant Number: 8055-00014B) funded by Innovation Fund Denmark, as well as FLSmidth A/S, Rockwool International A/S and Technical University of Denmark. Tero Luukkonen and Juho Yliniemi wish to acknowledge funding from the Academy of Finland (Grant Numbers 326291 and 322786, respectively).

Author Contributions IPS contributed to conceptualization, investigation, writing-original draft, writing-review and editing, and visualization. TL and JY contributed to conceptualization, writing- review and editing, and visualization. HS contributed to investigation, writing-review and editing, and visualization. AJD, MC, and LSJ contributed to writing- review and editing and visualization. AMK and V-VT contributed to writing- review and editing. PAJ contributed to writing- review and editing and visualization.

Data Availability The datasets generated during and/or analyzed during the current study are available from the corresponding author on reasonable request. Moreover, further information on raw data and calculations can be found in the supplementary material.

Declarations

Conflict of interest The authors declare that they have no known competing financial interests or personal relationships that could have appeared to influence the work reported in this paper.

Ethical Approval This article does not contain any studies with human participants or animals performed by any of the authors.

Open Access This article is licensed under a Creative Commons Attribution 4.0 International License, which permits use, sharing, adaptation, distribution and reproduction in any medium or format, as long as you give appropriate credit to the original author(s) and the source, provide a link to the Creative Commons licence, and indicate if changes were made. The images or other third party material in this article are

included in the article's Creative Commons licence, unless indicated otherwise in a credit line to the material. If material is not included in the article's Creative Commons licence and your intended use is not permitted by statutory regulation or exceeds the permitted use, you will need to obtain permission directly from the copyright holder. To view a copy of this licence, visit <http://creativecommons.org/licenses/by/4.0/>.

References

- Andrew RM (2019) Global CO₂ emissions from cement production, 1928–2018. *Earth Syst Sci Data* 11(4):1675–1710
- Abdollahnejad Z, Luukkonen T, Mastali M, Kinnunen P, Illikainen M (2019) Development of one-part alkali-activated ceramic/slag binders containing recycled ceramic aggregates. *J Mater Civ Eng* 31(2):04018386
- Provis JL, Bernal SA (2014) Geopolymers and related alkali-activated materials. *Annu Rev Mater Res* 44:299–327
- Emissions BZ (2016) Zero carbon industry plan: rethinking cement. Beyond Zero Emissions.
- Gartner E, Hirao H (2015) A review of alternative approaches to the reduction of CO₂ emissions associated with the manufacture of the binder phase in concrete. *Cem Concr Res* 78:126–142
- Luukkonen T, Abdollahnejad Z, Yliniemi J, Kinnunen P, Illikainen M (2018) One-part alkali-activated materials: a review. *Cem Concr Res* 103:21–34
- Criado M, Aperador W, Sobrados I (2016) Microstructural and mechanical properties of alkali activated Colombian raw materials. *Materials* 9(3):158
- Garcia-Lodeiro I, Palomo A, Fernández-Jiménez A, Macphee DE (2011) Compatibility studies between NASH and CASH gels. Study in the ternary diagram Na₂O–CaO–Al₂O₃–SiO₂–H₂O. *Cem Concr Res* 41(9):923–931
- Bernal SA, San Nicolas R, Myers RJ, de Gutiérrez RM, Puertas F, van Deventer JS, Provis JL (2014) MgO content of slag controls phase evolution and structural changes induced by accelerated carbonation in alkali-activated binders. *Cem Concr Res* 57:33–43
- Ren J, Sun H, Li Q, Li Z, Ling L, Zhang X, Wang Y, Xing F (2021) Experimental comparisons between one-part and normal (two-part) alkali-activated slag binders. *Constr Build Mater* 309:125177
- Luukkonen T, Yliniemi J, Abdollahnejad Z (2022) Alkali-activated dry-mix concretes. In: *Handbook of advances in Alkali-Activated Concrete*. Woodhead Publishing, pp 67–88
- Whviting J (1985) Manufacture of cement. United States Patent Office (US544706A) <https://patents.google.com/patent/US544706A>. Accessed 15 March 2022
- Adesanya E, Ohenoja K, Luukkonen T, Kinnunen P, Illikainen M (2018) One-part geopolymer cement from slag and pretreated paper sludge. *J Clean Prod* 185:168–175
- Ma C, Zhao B, Guo S, Long G, Xie Y (2019) Properties and characterization of green one-part geopolymer activated by composite activators. *J Clean Prod* 220:188–199
- Haruna S, Mohammed BS, Wahab MMA, Kankia MU, Amran M, Gora AUM (2021) Long-term strength development of fly ash-based one-part alkali-activated binders. *Materials* 14(15):4160
- Lemougna PN, Adediran A, Yliniemi J, Ismailov A, Levanen E, Tanskanen P, et al (2020) Thermal stability of one-part metakaolin geopolymer composites containing high volume of spodumene tailings and glass wool. *Cem Concr Compos* 114:103792
- Nematollahi B, Sanjayan J, Shaikh FUA (2015) Synthesis of heat and ambient cured one-part geopolymer mixes with different grades of sodium silicate. *Ceram Int* 41(4):5696–5704

18. Khale D, Chaudhary R (2007) Mechanism of geopolymerization and factors influencing its development: a review. *J Mater Sci* 42(3):729–746
19. Liew YM, Heah CY, Kamarudin H (2016) Structure and properties of clay-based geopolymer cements: a review. *Prog Mater Sci* 83:595–629
20. Lahoti M, Narang P, Tan KH, Yang EH (2017) Mix design factors and strength prediction of metakaolin-based geopolymer. *Ceram Int* 43(14):11433–11441
21. Sun Z, Vollpracht A (2018) Isothermal calorimetry and in-situ XRD study of the NaOH activated fly ash, metakaolin and slag. *Cem Concr Res* 103:110–122
22. Kosmatka SH, Kerkhoff B, Panarese WC (2002) Fly ash, slag, silica fume, and natural pozzolans. *Des Ctl Concr Mix* 13:57–72
23. CEN: European Committee for Standardization (2005) EN 196-3: methods of testing cement part 3—determination of setting times and soundness
24. Yang KH, Song JK, Ashour AF, Lee ET (2008) Properties of cementless mortars activated by sodium silicate. *Constr Build Mater* 22(9):1981–1989
25. Ma C, Long G, Shi Y, Xie Y (2018) Preparation of cleaner one-part geopolymer by investigating different types of commercial sodium metasilicate in China. *J Clean Prod* 201:636–647
26. Guo S, Ma C, Long G, Xie Y (2019) Cleaner one-part geopolymer prepared by introducing fly ash sinking spherical beads: properties and geopolymerization mechanism. *J Clean Prod* 219:686–697
27. Wang YS, Alrefaei Y, Dai JG (2021) Roles of hybrid activators in improving the early-age properties of one-part geopolymer pastes. *Constr Build Mater* 306:124880
28. Almakhadmeh M, Soliman AM (2021) Effects of mixing water temperatures on properties of one-part alkali-activated slag paste. *Constr Build Mater* 266:121030
29. Almakhadmeh M, Soliman AM (2019) Comparative analysis of reaction kinetics of one and two parts alkali activated slag. In: *Proceedings of the Annual Conference-Canadian society for civil engineering*
30. Ridditirud C, Chindaprasirt P, Pimraksa K (2011) Factors affecting the shrinkage of fly ash geopolymers. *Int J Miner Metall Mater* 18(1):100–104
31. Si R, Dai Q, Guo S, Wang J (2020) Mechanical property, nanopore structure and drying shrinkage of metakaolin-based geopolymer with waste glass powder. *J Clean Prod* 242:118502
32. Sanjuán MA, Argiz C (2012) The new European standard on common cements specifications EN 197–1: 2011. *Mater Constr* 62(307):425–430
33. Klun M, Bosiljkov V, Bokan-Bosiljkov V (2021) The relation between concrete, mortar and paste scale early age properties. *Materials* 14(6):1569
34. Zhang HY, Liu JC, Wu B (2021) Mechanical properties and reaction mechanism of one-part geopolymer mortars. *Constr Build Mater* 273:121973
35. Luukkonen T, Sreenivasan H, Abdollahnejad Z, Yliniemi J, Kantola A, Telkki VV, Kinnunen P, Illikainen M (2020) Influence of sodium silicate powder silica modulus for mechanical and chemical properties of dry-mix alkali-activated slag mortar. *Constr Build Mater* 233:117354
36. Sore SO, Messan A, Prud'Homme E, Escadeillas G, Tsobnang F (2020) Comparative study on geopolymer binders based on two alkaline solutions (NaOH and KOH). *JMMCE* 8(06):407
37. Caballero LR, Paiva MDDM, Fairbairn EDMR, Toledo RD (2019) Thermal, mechanical and microstructural analysis of metakaolin based geopolymers. *Mater Res*. <https://doi.org/10.1590/1980-5373-mr-2018-0716>
38. Luukkonen T, Sarkkinen M, Kemppainen K, Rämö J, Lassi U (2016) Metakaolin geopolymer characterization and application for ammonium removal from model solutions and landfill leachate. *Appl Clay Sci* 119:266–276
39. Kuo WT, Juang CU, Chen ZR (2020) Effect of burn joss paper ash on properties of ground-granulated blast furnace-based slag geopolymer. *Appl Sci* 10(14):4877
40. Ogirigbo OR, Black L (2016) Influence of slag composition and temperature on the hydration and microstructure of slag blended cements. *Constr Build Mater* 126:496–507
41. Ivanović MD, Kljajević LM, Nenadović M, Bundaleski N, Vukanac I, Todorović BŽ, Nenadović SS (2018) Physicochemical and radiological characterization of kaolin and its polymerization products. *Materiales de Construcción* 68(330):155
42. Chen K, Lin WT, Liu W (2021) Effect of NaOH concentration on properties and microstructure of a novel reactive ultra-fine fly ash geopolymer. *Adv Powder Technol* 32:2929
43. Kim B, Lee S (2020) Review on characteristics of metakaolin-based geopolymer and fast setting. *J Korean Ceram Soc* 57(4):368–377
44. Duxson P, Lukey GC, Separovic F, Van Deventer JSJ (2005) Effect of alkali cations on aluminum incorporation in geopolymeric gels. *Ind Eng Chem Res* 44(4):832–839
45. Duxson P, Provis JL, Lukey GC, Separovic F, van Deventer JSJ (2005) ²⁹Si NMR study of structural ordering in aluminosilicate geopolymer gels. *Langmuir* 21:3028–3036
46. Sreenivasan H, Adesanya E, Niu H, Perumal P, Kantola AM, Telkki VV, Huttula M, Cao W, Provis JL, Illikainen M, Kinnunen P (2021) Evidence of formation of an amorphous magnesium silicate (AMS) phase during alkali activation of (Na-Mg) aluminosilicate glasses. *Cem Concr Res* 145:106–464

Publisher's Note Springer Nature remains neutral with regard to jurisdictional claims in published maps and institutional affiliations.

Authors and Affiliations

Isabel Pol Segura¹  · Tero Luukkonen² · Juho Yliniemi² · Harisankar Sreenivasan² · Anne Juul Dam¹ · Lars Skaarup Jensen³ · Mariana Canut³ · Anu M. Kantola⁴ · Ville-Veikko Telkki⁴ · Peter Arendt Jensen¹

¹ Department of Chemical and Biochemical Engineering, Technical University of Denmark, 2800 Kgs. Lyngby, Denmark

² Department of Fibre and Particle Engineering Research Unit, University of Oulu, 90570 Oulu, Finland

³ Department of Research and Development, FLSmidth, 2500 Valby, Denmark

⁴ NMR Research Unit, Faculty of Science, University of Oulu, P.O. Box 3000, 90014 Oulu, Finland